Indonesian Physical Review

Volume 5 Issue 3, September 2022

P-ISSN: 2615-1278, E-ISSN: 2614-7904

The effect of additional iron sand on the crystal size and strain of ZnO

Lorna[1*], Inayatul Mutmainna[1], Dahlang Tahir[1] and Paulus L Gareso[1*]

[1]Department of Physics, Faculty of Mathematics and Natural Sciences, Hasanuddin University, Jl. Perintis Kemerdekaan km. 10, Tamalanrea Makassar 90245, Indonesia.

Corresponding author E-mail: pgareso@fmipa.unhas.ac.id, lornarlansyah.96@gmail.com

Article Info

Article info:

Received: 06-07-2022

Revised: 24-07-2022

Accepted: 02-08-2022

Keywords:

Iron (Fe); ZnO Nanoparticle; X-Ray Diffraction

How To Cite:

Lorna, I. Mutmainna, D. Tahir and Paulus L. Gareso "The Effect of Additional Iron Sand on The Crystal Size and Strain Of Zno", Indonesian Physical Review, vol. 5, no. 3, p, 168-176, 2022

DOI:

https://doi.org/10.29303/ipr.v5i3.178

Abstract

This study observed the effect of the addition of iron (Fe) doping on the characteristics of Zinc Oxide (ZnO) nanoparticles.$Zn_{(1-x)}Fe_{(x)}$ with various concentration of x = 0, 2, 4, 6, 8, and 10% was prepared by coprecipitation method using Sodium Hydroxide and Hydrogen Chloride. The effect of adding Fe doping on ZnO was characterized using X-ray Diffraction (XRD) to determine the crystal structure, size, and strain. The analysis result confirmed the absence of additional impurity peaks in the ZnO nanoparticles. Fe doping affects the Zn lattice structure. X-ray diffraction (XRD) study confirms the crystalline Hexagonal structure. Crystal size analysis using Debye Scherrer, UDM, and Halder-Wagner method obtained varying crystal sizes with variations in the concentration of Fe ranging from 19.89-44.72 nm. The crystal size and strain obtained from the Debye Scherrer method are smaller.

Introduction

ZnO is a semiconductor material having various applications [1]. ZnO in nanometer dimensions has unique physical properties, which are strain and crystal size that can be adjusted by varying the synthesis parameters. The parameters can be confirmed using X-ray Diffraction and can be determined indirectly using analytical methods such as Debye Scherrer, UDM, and Halder-Wagner [2]. ZnO's physical and chemical properties can be modified by including impurities such as metals and non-metals. Various types of metal elements have been used to doped ZnO such as ZnO doped Cu, Fe, Y, Mn, Ni, Ag, showed a hexagonal wurtzite structure, where the distribution of metal ions greadly affects the microstructural properties of material [3-9]. ZnO nanoparticles will show significant changes in properties

when doped with appropriate elements and depending on the synthesis method [10]. The main drawback of ZnO semiconductors is the low charge separation efficiency.

In recent years, metal oxide nanoparticles such as ZnO doped metal transition have been widely investigated due to their structural, optical, and photocatalysts. Iron (Fe), as one of the transition metals, shows ferromagnetic properties [11]. Nanometer-sized ferromagnetic materials have super-paramagnetic properties with high saturation magnetization [12]. The ferrite material is contained in natural iron sand [13]. Utilization of iron sand has been widely used in concrete mixtures [14], and anti-bacterial filters [15-17].

The use of transition metals as ZnO doping was identified as a promising candidate. Among the transition metals, Fe has a large effective magnetic moment. This paper used the coprecipitation technique to synthesize the iron from the natural iron sand. The effect of adding iron to ZnO nanoparticles was studied using X-ray diffraction to obtain the crystal structures and the strain.

Experimental Method

Magnetic Material (MM) is separated from iron sand using a permanent magnet. The magnetic material was ground to 200 mesh and then washed using a 12 M HCl 37% for a 1:2 ratio. 50 ml of 6.5 M NH_3 16% added into one mmol Polyethylene Glycol (PEG 6000 99%). The MM obtained was put into the NH_3/PEG solution while stirring for 90 minutes until a precipitate was formed. The precipitate was then washed using aquabidest until it reached pH 7. The results were heated in an oven at 100^{o}C for 5 hours to form a powder [12].

Dissolve 2.19 g of Zinc acetate dehydrate 99% into 100 ml of aquabidest. Adding the synthesis of iron sand to the solution in a ratio of 0-8% ($Zn_{1-x}Fe_xO$; x = 0, 0.02, 0.04, 0.06, 0.08 and 0.1). 0.3 M NaOH solution was added using the titration method into the precursor solution until it reached pH 12, stirred for 2 hours, and formed a precipitate. The precipitate was then filtered and washed using aquabidest and ethanol. Then dried in the oven at 100^{o}C for 6 hours. The resulting powder was calcined in the furnace at a temperature of 600^{o}C for 2 hours, and then ground to produce finer particles [18]. For each doping measure, x=0, 0.02, 0.04, 0.06, 0.08 and 0.1 are symbolized by ZF, ZF_2, ZF_4, ZF_6, ZF_8 and ZF_{10}. The samples were characterized using XRD.

Result and Discussion

XRD (X-ray Diffraction) analysis was performed to determine the crystal structure and size of the sample $Zn_{x-1}Fe_xO$ (x = 0, 0,02, 0,04, 0,06, 0,08, and 0,1). The diffraction patterns of undoped ZnO (ZF) and Fe doped ZnO (ZF_2, ZF_4, ZF_6, ZF_8 dan ZF_{10}) are depicted in Figure 1. The observations were made at an angle range of 2θ=28°-73°. Overall the diffraction peaks form a hexagonal structure for samples with various variations corresponding to the standard peaks of ZnO (JCPD Card no: 01-075-0576). The diffraction peaks were observed at 31.91°, 34.58°, 36.41°, 47.70°, 56.74°, 63.01°, 68.10°, and 69.24°. These peaks correspond to the diffraction plane of (100), (002), (101), (102), (110), (103), (112), and (201), respectively which is show in table 1. In addition, the primary diffraction peak is observed at the (101) plane, indicating the growth direction of the ZnO nanoparticles doped iron in (101) plane.

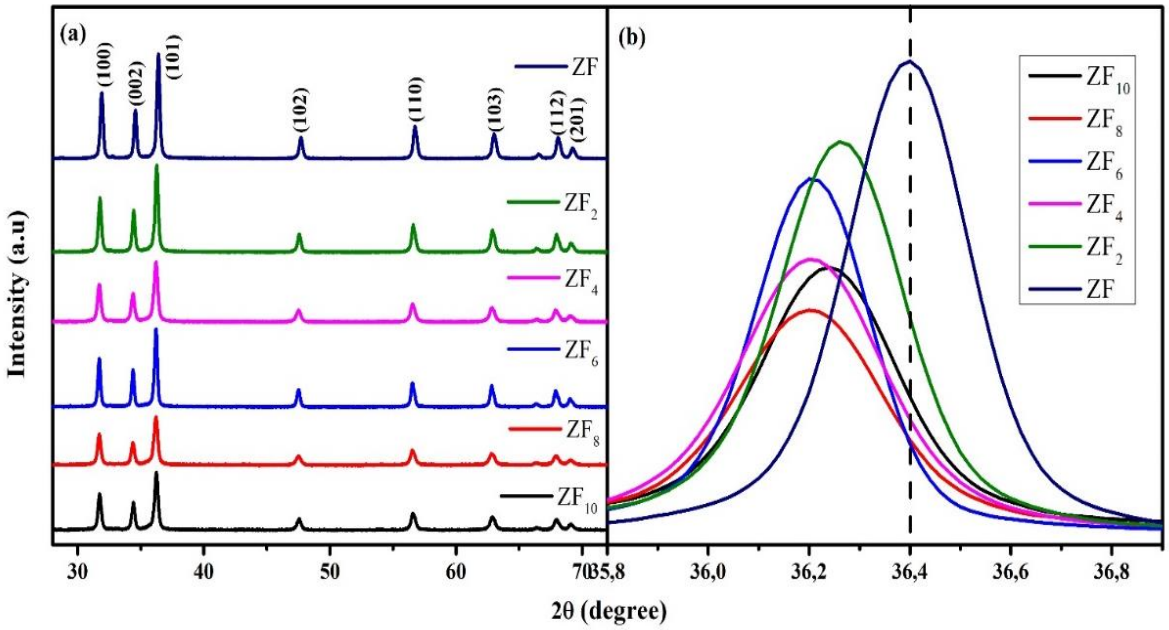

Figure 1. (a) XRD pattern of ZnO nanoparticles with Fe doping variation, (b) Peak shift in hkl (101).

Tabel 1. Value of (hkl) plane and 2θ (degree) (JCPD Card no: 01-075-0576).

No.	(hkl) plane	2θ (degree)
1	(100)	31.91
2	(002)	34.58
3	(101)	36.41
4	(102)	47.70
5	(110)	56.74
6	(103)	63.01
7	(112)	68.10
8	(201)	69.24

The results explain that the sample doped with Fe has a decrease in peak intensity, showing a reduction in the crystallinity of the nanoparticles. The higher the crystal size, the higher and narrower the peak formed [19] but retained its structure [20]. In addition, there was a shift of the peak to a smaller angle in each Fe doped sample, indicating that the Fe dopant had been substituted into ZnO and partially replaced the position of the Zn^{2+} ion. This is due to the effect of different ionic radii, where Fe^{2+} ions are more prominent than Zn^{2+} ions and show that the ZnO structure gradually degrades [7,18]. The peak indicates that the synthetic material is monophasic in all Fe content because there is no additional peak [21]. Bragg's law is used to study crystals from x-ray diffraction, where the greater the scattering angle, the smaller the distance between the fields, and vice versa [18]. The relationship between crystal size and the width of the x-ray diffraction peak is based on the Scherrer formula, namely [22]:

$$D = \frac{k\lambda}{\beta \cos\theta} \quad (1)$$

$$\beta = \sqrt{FWHM_{sampel} - FWHM_{standar}} \quad (2)$$

where D is the crystal size in nanometers, λ is the wavelength, the Bragg angle θ, β is the width of the diffraction peak at half the maximum of the test sample $FWHM_{sampel}$.

The crystal size of ZF before doping was 25.12 nm, then the crystal size obtained from adding Fe ions (2%, 4%, 8%, and 10%) through the Debye Scherrer equation was 20.03 nm – 24.63 nm, which showed a decrease in crystal size. This result is due to an increase in lattice disturbance and strain caused by Fe^{2+} substitution, which suppresses the growth of ZnO crystal grains [9,11] and is associated with decreased nucleation and growth rate because the ionic radius of Fe^{2+} is higher than that of Zn^{2+} ion [9,18]. An increase in crystal size was also observed but not substantially [11]. The strain value is inversely proportional to the crystal size value. The most prominent strain was obtained in the ZF_4 sample and the smallest in the ZF_6 sample. The overall results of the calculation of crystal size and strain are summarized in table 2.

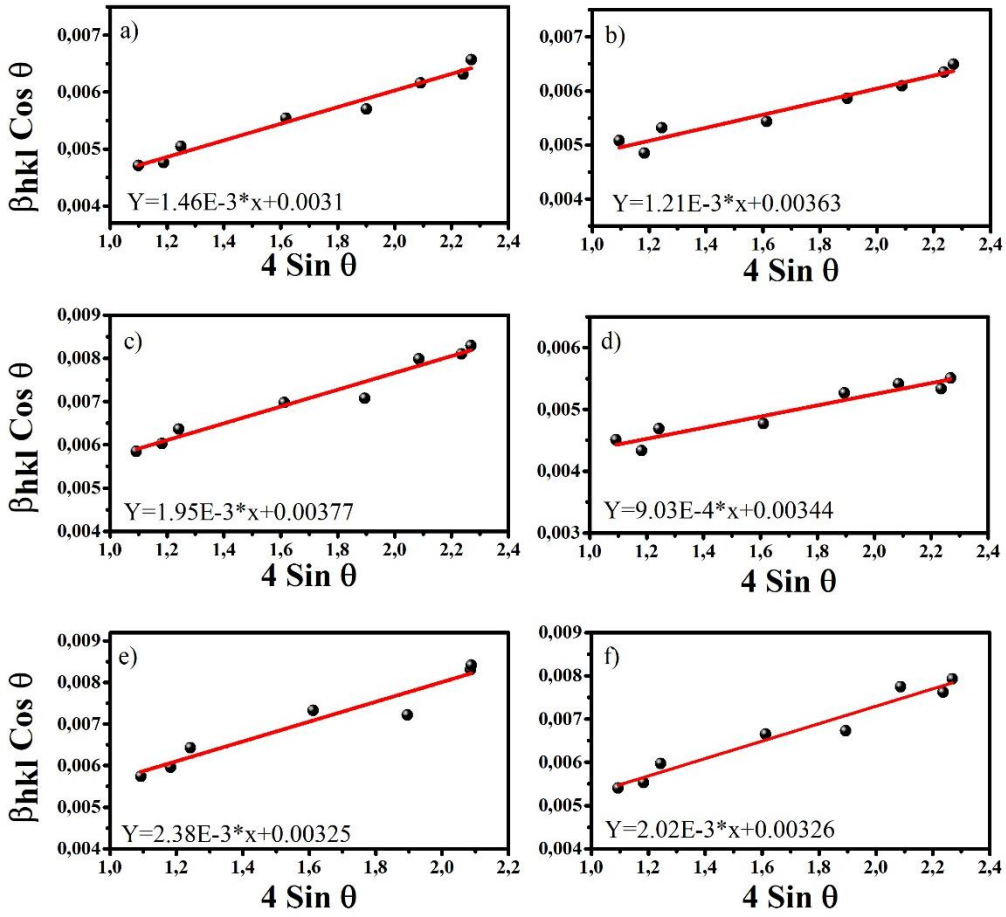

Figure 2. The plot of W-H method for a) ZF, b) ZF_2, c) ZF_4, d) ZF_6, e) ZF_8 and f) ZF_{10}.

Meanwhile, in the Williamson-Hall method, the crystal size and micro-strain of the diffraction pattern are used with the following equation:[23]

$$\beta_{hkl} \cos\theta = \frac{k\lambda}{D} + 4\varepsilon \sin\theta \quad (3)$$

$$\varepsilon = \frac{\beta_{hkl}}{4 \tan\theta} \quad (4)$$

where β_{hkl} is full width at half maximum (FWHM), ε is lattice strain. The least-squares fit is used in $\beta_{hkl}\cos\theta$ versus $4\sin\theta$ to measure the slope and the intercept to calculate D and ε [24].

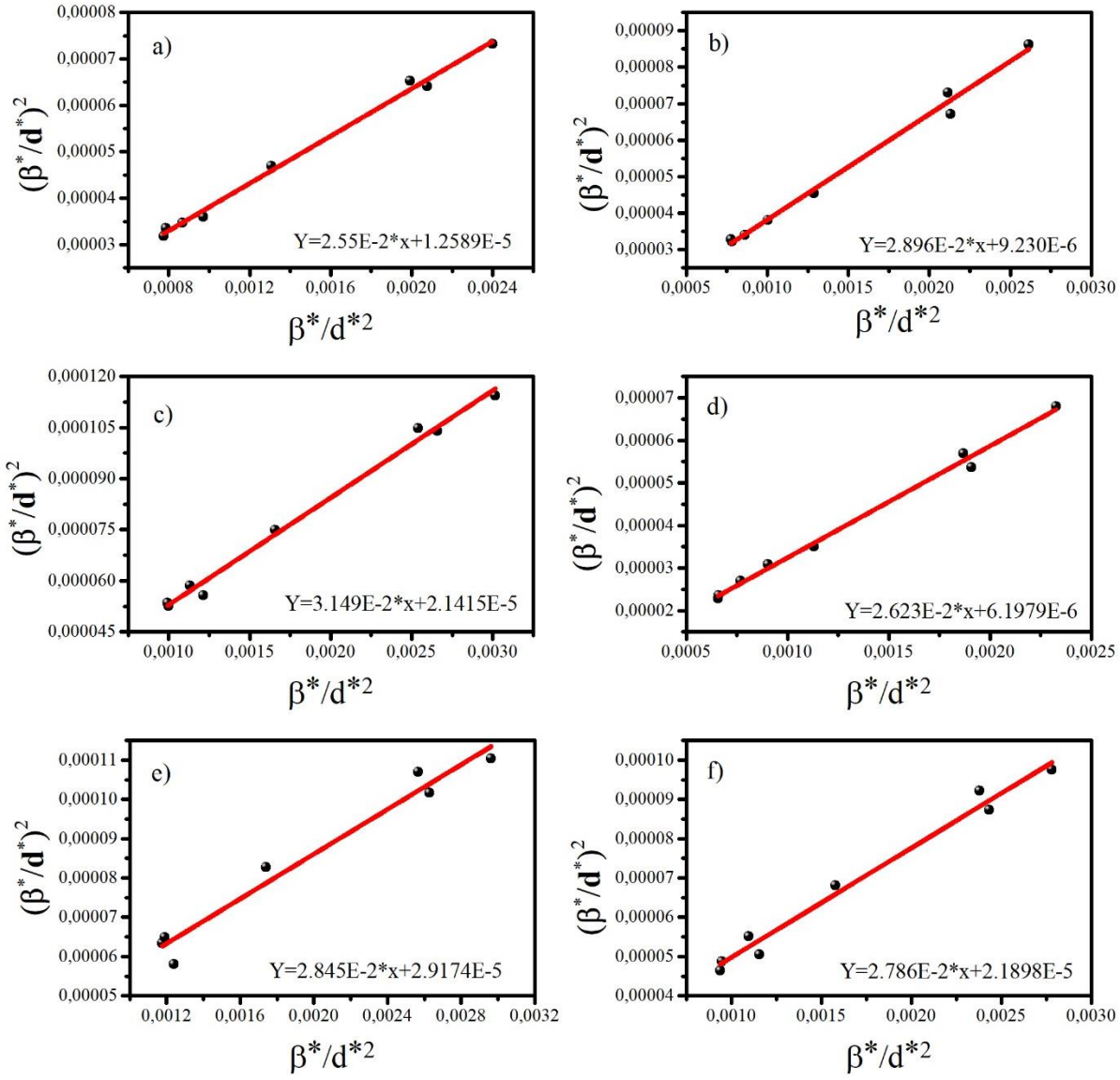

Figure 3. The plot of H-W method for a) ZF, b) ZF_2, c) ZF_4, d) ZF_6, e) ZF_8 and f) ZF_{10}.

The UDM (Uniform Deformation Model) representation where the x-axis is 4sinθ and the y-axis is β_{hkl}cosθ is shown in Figure 2a, 2b, 2c, 2d, 2e, and 2f for ZF, ZF_2, ZF_4, ZF_6, ZF_8 and ZF_{10} which shows a good fit line on the positive slope. The results show the compressive strain associated with the lattice increase that may occur in calculating the lattice parameters. The values of D and ε are calculated from the intercept and slope obtained by plotting 4sinθ for β_{hkl}cosθ, respectively. The slope of the plot is associated with the increase in strain given by the larger ionic radious of Fe ions than Zn ions esulting in lattice expansion. According to Williamson-Hall, the crystal size decreases with the presence of doping, which is shown in

table 2. In addition, compared with the Debye-Scherrer equation, the crystal size according to Willamson-Hall is larger. Positive skewness implies strain occurrence in all synthesized materials and reduced size, indicating dislocations in the crystal lattice [3]. This equation is known from the uniform deformation model because the microstrain should be the same in all crystallographic orientations [25]. In the W-H plot, the diffraction domain is isotropic, representing a uniform deformation model for all crystallographic directions [26].

According to Halder-Wagner, the relationship between crystal size and lattice strain is: [27]

$$\left(\frac{\beta^*}{d^*}\right)^2 = \frac{1}{D}\left(\frac{\beta^*}{d^{*2}}\right) + \left(\frac{\varepsilon}{2}\right)^2 \quad (5)$$

The H-W interpretation of the straight line (slope) between the graph plot representing the x-axis is $\left(\frac{\beta^*}{d^{*2}}\right)$ and the y-axis is $\left(\frac{\beta^*}{d^*}\right)^2$ as shown in Figure 3a, 3b, 3c, 3d, 3e, and 3f for ZF, ZF_2, ZF_4, ZF_6, ZF_8 and ZF_{10}. The average value of crystal size is obtained from the straight-line slope and the intercept of the plot gives the intrinsic strain. This method assumes that the peak widening is the full half-maximum width [2]. The crystal size obtained varies from the doping variation with a value larger than the Debye Scherrer method and slightly smaller than the W-H method. The lattice strain obtained is larger than other methods. The increase in strain values is thought to be due to the diffraction pattern's low and middle angle contribution associated with lattice dislocations, which expand the reflection peak at lower angles. This method has the advantage of giving more weight to the low and middle angle ranges [27].

All the average sizes and strains calculated by different methods are shown in table 2. From table 2, it is found that the sizes obtained are decreasing and increasing in value. The increased strain value in the case of the H-W method is due to the fact that the value of the low and middle angles is important. Meanwhile, the W-H method shows a slightly higher value which is also associated with the Fe doping effect. The strain values using the H-W method were very different from those calculated by the Debye Scherrer and W-H methods for each of these nanocrystals. Almost the same value with the Fe doping effect where the ionic radius of Fe is larger than Zn [2,22]. Because of these consideations, it can be attributed that doping affects the strain and crystal size.

Table 2. The crystal parameters of Fe doped ZnO nanoparticles with different models.

No.	Sample	FWHM (deg)	Debye Scherrer		Williamson-Hall (UDM)		Halder-Wagner	
			D (nm)	$\varepsilon^*(10^{-3})$	D (nm)	$\varepsilon^*(10^{-3})$	D (nm)	$\varepsilon^*(10^{-3})$
1	ZF	0.362	25.12	0.81	44.72	1.46	39.21	7.09
2	ZF_2	0.367	24.63	0.82	38.19	1.21	34.53	6.07
3	ZF_4	0.457	19.89	1.02	36.77	1.95	31.75	9.25
4	ZF_6	0.321	25.28	0.71	40.30	1.09	38.12	4.98
5	ZF_8	0.448	20.03	0.92	42.66	2.38	35.14	10.80
6	ZF_{10}	0.433	21.12	0.97	42.53	2.02	35.89	9.35

Conclusion

$Zn_{(1-x)}Fe_{(x)}O$ nanoparticles were successfully prepared using the coprecipitation method with various concentration x = 0, 2, 4, 6, 8, dan 10% has been studied to obtained the crystalline size and intrinsic strain from XRD peak. X-ray diffraction (XRD) study confirms the crystalline

Hexagonal structure. Debye Scherrer, Williamson-Hall (W-H), Halder-Wagner (H-W) methods have been investigated. The average particle size determined is approximately 19.89-44.72 nm. The crystal size and strain obtained from the Debye Scherrer method are smaller.

References

[1] A. T. Ravichandran and R. Karthick, "Enhanced photoluminescence, structural, morphological and antimicrobial efficacy of Co-doped ZnO nanoparticles prepared by Co-precipitation method," *Results Mater.*, vol. 5, no. January, p. 100072, 2020.

[2] D. Nath, F. Singh, and R. Das, "X-ray diffraction analysis by Williamson-Hall , Halder-Wagner and size-strain plot methods of CdSe nanoparticles- a comparative study," *Mater. Chem. Phys.*, vol. 239, no. August 2019, p. 122021, 2020.

[3] Siddiqui V.U, *et al.*, "Optimization of Facile Synthesized ZnO / CuO," Catalyst, 11, 1509, 2021.

[4] O. D. K. Szostak and M. K. M. Banach, "Synthesis of - Fe3O4 / ZnO nanoparticles and their application for the photodegradation of anionic and cationic dyes," *Int. J. Environ. Sci. Technol.*, vol. 18, no. 3, pp. 561–574, 2021.

[5] J. Hu, W. Ma, Y. Pan, Z. Cheng, S. Yu, and J. Gao, "Chemosphere Insights on the mechanism of Fe doped ZnO for tightly-bound extracellular polymeric substances tribo-catalytic degradation: The role of hydration layers at the interface," *Chemosphere*, vol. 276, p. 130170, 2021.

[6] S. Sujinnapram and S. Wongrerkdee, "Synergistic effects of structural , crystalline , and chemical defects on the photocatalytic performance of Y-doped ZnO for carbaryl degradation," *J. Environ. Sci.*, vol. 124, pp. 667–677, 2023.

[7] A. Zamani, M. S. Sadjadi, A. Mahjoub, M. Yousefi, and N. Farhadyar, "Synthesis , characterization and investigation of photocatalytic activity of - ZnMnO3 / Fe3O4 nanocomposite for degradation of dye Congo red under visible light irradiation," *Int. J. Ind. Chem.*, vol. 11, no. 4, pp. 205–216, 2020.

[8] M. N. Siddique, T. Ali, A. Ahmed, and P. Tripathi, "Enhanced electrical and thermal properties of pure and Ni substituted ZnO Nanoparticles," *Nano-Structures and Nano-Objects*, vol. 16, pp. 156–166, 2018.

[9] J. Zhang *et al.*, "A synergistic boost of photo-activity of ZnO for photocatalytic degradation of methylene blue by Ag decoration and Fe doping," *Mater. Lett.*, vol. 286, no. 3, p. 129250, 2021.

[10] K. Liu, Y. Li, F. Wang, J. Ren, and H. Xie, "Modeling and experimental study of multiple factors on mechanical strength of iron sand modified cement mortars," *Constr. Build. Mater.*, vol. 178, pp. 144–152, 2018.

[11] A. Nauman *et al.*, "Structural and magnetic properties of highly Fe-doped ZnO nanoparticles synthesized by one-step solution plasma process," *J. Alloys Compd.*, vol. 853, p. 157153, 2021.

[12] P. Sebayang and M. Properties, "The synthesization of Fe 3 O 4 magnetic nanoparticles

based on natural iron sand by co- precipitation method for the used of the adsorption of Cu and Pb ions" Journal of Physics: 8th International Conference on Physics and its Applications (ICOPIA), no. 1-6, vol. 776, 2020.

[13] A. You, M. A. Y. Be, and I. In, "Characterization of magnetic content from Puntaru Beach iron sand Characterization of Magnetic Content from Puntaru Beach Iron Sand," vol. 020026, no. June, 2021.

[14] M. Bhargav, S. Abdul, R. Syed, and A. Khadar, "Materials Today : Proceedings Characterization of fibre R . C . Beam made with partial replacement of sand with iron ore," *Mater. Today Proc.*, vol. 45, pp. 6590–6595, 2021.

[15] A. Mažeikienė, R. Vaiškūnaitė, and J. Šarko, "Jo ur na l P of," *Sci. Total Environ.*, p. 142915, 2020.

[16] Y. Lai, J. Yu, S. Liu, J. Liu, R. Wang, and B. Dong, "Experimental study to improve the mechanical properties of iron tailings sand by using MICP at low pH," *Constr. Build. Mater.*, no. xxxx, p. 121729, 2020.

[17] N. Lambert, P. Van Aken, R. Van den Broeck, and R. Dewil, "Adsorption of phosphate on iron-coated sand granules as a robust end-of-pipe purification strategy in the horticulture sector," *Chemosphere*, vol. 267, p. 129276, 2021.

[18] S. Roguai and A. Djelloul, "Structural , microstructural and photocatalytic degradation of methylene blue of zinc oxide and Fe-doped ZnO nanoparticles prepared by simple coprecipitation method," *Solid State Commun.*, vol. 334–335, no. May, p. 114362, 2021.

[19] M. Rianna *et al.*, "The effect of Mg-Al additive composition on microstructure , magnetic properties , and microwave absorption on BaFe 12 À 2x Mg x Al x O 19 (x = 0 – 0 . 5) material synthesized from natural iron sand," *Mater. Lett.*, vol. 256, p. 126612, 2019.

[20] F. A. Jan, R. Ullah, N. Ullah, and M. Usman, "Exploring the environmental and potential therapeutic applications of Myrtus communis L . assisted synthesized zinc oxide (ZnO) and iron doped zinc oxide (Fe-ZnO) nanoparticles," *J. Saudi Chem. Soc.*, vol. 25, no. 7, p. 101278, 2021.

[21] T. M. Bawazeer, M. S. Alsoufi, M. Shkir, B. M. Al-Shehri, and M. S. Hamdy, "Excellent improvement in photocatalytic nature of ZnO nanoparticles via Fe doping content," *Inorg. Chem. Commun.*, vol. 130, p. 108668, 2021.

[22] I. Nkurikiyimfura, Y. Wang, and E. Nshingabigwi, "Temperature-dependent magnetic properties of magnetite nanoparticles synthesized via coprecipitation method," vol. 846, 2020.

[23] L. M. Jose, R. S. A. Raj, D. Sajan, and A. Aravind, "Adsorption and photocatalytic activity of biosynthesised ZnO nanoparticles using Aloe Vera leaf extract Adsorption and photocatalytic activity of biosynthesised ZnO nanoparticles using Aloe Vera leaf extract," pp. 0–15, 2014.

[24] P. Kushwaha and P. Chauhan, "Microstructural evaluation of iron oxide nanoparticles at different calcination temperature by Scherrer , Williamson-Hall , Size-Strain Plot and Halder-Wagner methods," 2021.

[25] A. K. Prajapati and M. K. Mondal, "Novel green strategy for CuO–ZnO–C nanocomposites fabrication using marigold (Tagetes spp .) flower petals extract with and without CTAB treatment for adsorption of Cr (VI) and Congo red dye," *J. Environ. Manage.*, vol. 290, no. November 2020, p. 112615, 2021.

[26] S. Castro-lopes *et al.*, "Influence of pH on the structural and magnetic properties of Fe-doped ZnO nanoparticles synthesized by sol gel method," vol. 109, no. September, 2020.

[27] M. K. Kamil and K. A. Jasim, "Investigation the Crystalline Size and Strain of Perovskite (YBa 2 Cu 3 O 6 + σ) by variant method," no. 8719, pp. 8719–8723, 2020.